Original Article

Sensitivity and specificity of computed tomography hypodense sign when differentiating pulmonary inflammatory and malignant mass-like lesions

Bin-Jie Fu[1#], Zhuo-Ma Lv[1,2#], Fa-Jin Lv[1], Wang-Jia Li[1], Rui-Yu Lin[1], Zhi-Gang Chu[1]

[1]Department of Radiology, The First Affiliated Hospital of Chongqing Medical University, Chongqing, China; [2]Department of Radiology, The Second People's Hospital of Yubei District, Chongqing, China

Contributions: (I) Conception and design: ZG Chu; (II) Administrative support: FJ Lv; (III) Provision of study materials or patients: ZG Chu, FJ Lv; (IV) Collection and assembly of data: BJ Fu, ZM Lv, WJ Li, RY Lin; (V) Data analysis and interpretation: BJ Fu, ZM Lv; (VI) Manuscript writing: All authors; (VII) Final approval of manuscript: All authors.

[#]These authors contributed equally to this work.

Correspondence to: Zhi-Gang Chu. Department of Radiology, The First Affiliated Hospital of Chongqing Medical University, 1 Youyi Road, Yuanjiagang, Yuzhong, Chongqing 400016, China. Email: chuzg0815@163.com.

Background: Hypodense sign (HyS) reportedly is associated with pulmonary fungal infection, while it also common in many non-fungal lesions. This study aims to determine the significance of a HyS presented on contrast-enhanced computed tomography (CECT) when distinguishing pulmonary inflammatory from malignant mass-like lesions.

Methods: From January 2013 to January 2021, we retrospectively evaluated the clinical and computed tomography (CT) data of patients with pathologically confirmed pulmonary inflammatory lesions (ILs) and malignant lesions (MLs). We analyzed and compared the CT features of the HyS in MLs and ILs, and then evaluated whether the HyS helped to differentiate MLs and ILs.

Results: There were significant differences in age and tumor markers between patients with ILs and MLs (both P<0.05). Compared with that in MLs, the occurrence of the HyS in ILs was higher (62.81% *vs.* 28.81%; P<0.0001). In ILs, more HyS were single, round or oval, well-defined, and had lower enhancement (ΔCT). Logistic regression analysis revealed that an ill-defined boundary, peripheral fibrosis, presence of a well-defined HyS, and a ΔCT value of the HyS <9.5 Hounsfield units (HU) were independent indicators for predicting ILs. After including the HyS CT features, the area under the curve (AUC) of the model predicting ILs increased from 0.953 to 0.986 with a sensitivity of 96.03% and a specificity of 94.03% (P=0.0027).

Conclusions: The HyS is more common in ILs than in MLs. A single, regular, and well-defined HyS with a ΔCT value of <9.5 HU on CECT is highly suggestive of ILs. Combining the HyS with other morphological features could improve the diagnosis accuracy of pulmonary mass-like lesions.

Keywords: Inflammation; hypodense sign (HyS); differential diagnosis; tomography; X-rays

Submitted Aug 26, 2021. Accepted for publication Jun 06, 2022.
doi: 10.21037/qims-21-851
View this article at: https://dx.doi.org/10.21037/qims-21-851

Introduction

Lung cancer is one of the cancers with the highest morbidity and mortality globally (1-3). The treatment and prognosis of patients greatly depend on accurate diagnosis and staging. Misdiagnosis not only delays the patient's treatment, but also impacts prognosis and recovery (4). Imperfect noninvasive diagnostic performance leads to a high frequency of non-therapeutic resection and missed treatment opportunities in lung cancers (5-7). In contrast, because the risk of malignancy increases with the size of localized pulmonary lesions, mass-like inflammatory lesions (ILs) are sometimes misdiagnosed as lung cancers (8), which can result in unnecessary surgical resection. Therefore, improving the ability to distinguish between pulmonary inflammatory and malignant lesions (MLs) is critical for directing further treatment.

Contrast-enhanced computed tomography (CECT) is a useful noninvasive diagnostic method for patients with pulmonary mass-like lesions to provide valuable information for diagnosis and differential diagnosis (9-11). Most previous studies on differentiating pulmonary benign and MLs have been based on computed tomography (CT) morphological features or CT texture analysis (12-16). Although some differences have been found between ILs and MLs, no reliable features have been determined for diagnosing benign lesions. Therefore, further study is needed to improve techniques differentiating between ILs and MLs. Previous studies have revealed that internal hypodensity [hypodense sign (HyS)] in pulmonary consolidation or nodules on CT images is highly indicative of fungal infection in immunocompromised patients (17-19). Nevertheless, in clinical practice, this sign has also been found in some patients with other pulmonary inflammatory (non-fungal infection) masses or MLs. However, it has not been clarified whether this sign is different between non-fungal ILs and MLs and whether it could improve their differential diagnosis.

Our study retrospectively included 198 and 235 patients with pathologically confirmed pulmonary mass-like ILs and MLs (≥3 cm), respectively. We evaluated their data to determine whether the HyS presenting on CECT could differentiate these lesions. The patients' clinical and CT data were collected and evaluated. The CT features of lesions and the HyS in MLs and ILs were comprehensively analyzed and compared, and the values of the HyS for improving differential diagnosis were evaluated. We present the following article in accordance with the STARD reporting checklist (available at https://qims.amegroups.com/article/view/10.21037/qims-21-851/rc).

Methods

The study was conducted in accordance with the Declaration of Helsinki (as revised in 2013). It was approved by the Ethics Committee of the First Affiliated Hospital of Chongqing Medical University (No. 2019-062), which waived the requirement for informed consent for this retrospective study. The data of patients who underwent CECT with pulmonary ILs and MLs confirmed by pathology were retrospectively collected. The clinical data of patients with ILs and MLs were compared, and the CT manifestations of ILs and MLs and characteristics of the HyS in lesions on plain CT and CECT were blindly observed and compared. In addition, the diagnostic efficacy of the HyS in differentiating ILs and MLs was also examined. More details of the diagnostic study had been previously reported in detail in the research of Fukukura *et al.* (20).

Patients

A retrospective study was consecutively performed from January 2013 to January 2021, including patients with pathologically confirmed ILs and lung cancers manifested as localized pulmonary lesions. The inclusion criteria were as follows: (I) patients underwent CECT examination; (II) the largest diameter of the lesion was ≥3 cm; and (III) the interval between CT examination and operation was less than 2 weeks. Patients who met the following conditions were excluded: (I) the ILs were confirmed as a fungal infection (to meet the purpose of this study); (II) the pathological diagnosis was unclear; and (III) the patient had a combination of other diffuse pulmonary diseases that affected the observation of lesions. Finally, 433 patients with 435 lesions (inflammatory group: 198 patients with 199 lesions; malignant group: 235 patients with 236 lesions) were enrolled in this study (*Figure 1*). Besides the gender and age of the patients, the collected clinical data included smoking history, family history, and clinical manifestations. Laboratory data included routine bloodwork , inflammatory markers, and tumor markers.

CT protocol

Patients were examined with a SOMATOM Definition Flash (Siemens Healthineers, Erlangen, Germany),

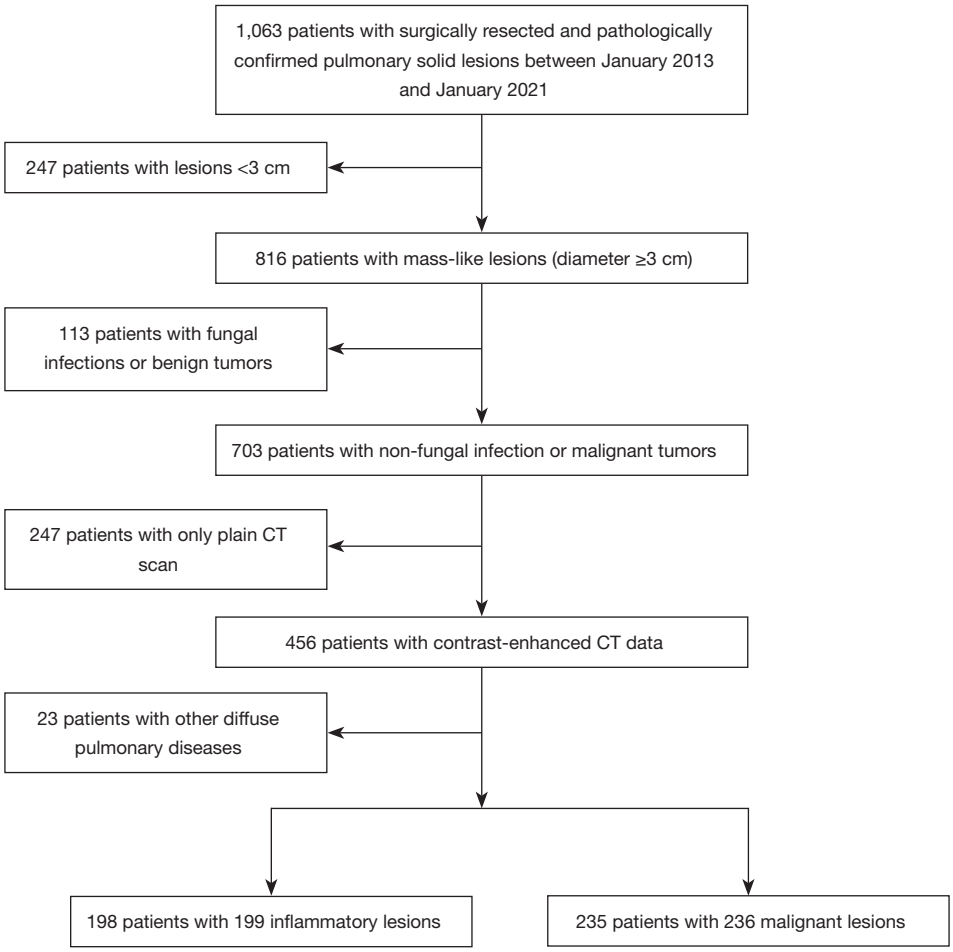

Figure 1 Flow diagram for the inclusion and exclusion of patients. CT, computed tomography.

Discovery CT 750 HD (GE Healthcare, Milwaukee, WI, USA), and SOMATOM Force (Siemens Healthineers, Germany) CT scanner. All patients were scanned in a supine position with both upper limbs raised close to the head. Breath-holding exposure was performed after deep inspiration. The parameters were as follows: tube voltages, 100–130 kVp; tube current, 80–250 mAs (using automatic tube current modulation technology); pitch, 0.9–1; rotation time, 0.5–0.6 s; slice thickness and slice spacing: 5 mm; matrix: 512×512; and reconstruction algorithm, medium-sharp algorithm, or standard algorithm. The acquisition range was from the level of thoracic entrance to the inferiority of the costophrenic angles. Subsequently, all patients underwent contrast-enhanced scans with 70–100 mL (1.5 mL/kg) of nonionic iodinated contrast material at a flow rate of 3–3.5 mL/s followed by 30–50 mL saline solution at the same injection rate. The automatic bolus tracking method was used to detect the ascending aorta with a threshold of 150 Hounsfield units (HU) followed by a delay of 6 seconds before scanning. A delayed phase was performed at the 150th second after the injection of the contrast agent. After enhancement examination, no severe adverse reactions occurred among all patients included in this study. All the images were transferred to the archiving and communication system.

Among the 433 patients, the lesions in 159 patients (36.7%) were found with a plain CT scan. They underwent further CECT examination with an interval of 41.5±72.4 days (range, 1 to 347 days) between these 2 CT scans. A total of 47 (29.6%) of these cases received anti-inflammatory treatment during this period. In contrast, enhanced CT was performed directly based on patients' clinical symptoms (176 cases, 40.6%) and abnormal findings (98, 22.6%) revealed by chest X-ray photography.

Imaging analysis

Two senior radiologists specializing in chest imaging independently analyzed the CT images of all patients without knowing the pathological results. The CT manifestations of the lesions were observed with the window setting of the lung (width, 1,200–1,600 HU; level, −500 to −700 HU) and mediastinum (width, 350–450 HU; level, 20–40 HU). Divergent results from the 2 radiologists were agreed upon after discussion.

The imaging evaluation was carried out considering the following aspects:

(I) CT characteristics of lesions: (i) size (mean value of the longest diameter and the perpendicular diameter); (ii) distribution; (iii) lesion shape: patchy, oval/round, lobulated (lesions with undulating contour), and irregular (the shape cannot be described above); (iv) boundary and margin (smooth, spiculated, and ill-defined); (v) peripheral changes [ground-glass opacities (GGO), fibrosis, halo signs, nodules, or consolidation]; (vi) pleural changes (pleural traction or thickening); and (vii) lymph nodes (enlargement of the mediastinal or hilar lymph node).

(II) The HyS: (i) to determine whether there was a HyS on the standard mediastinal window (width, 350–450 HU; level, 20–40 HU) or narrow mediastinal window (width, 110–140 HU; level, 14–40 HU) of plain CT and CECT; (ii) the CT features of the HyS: number (single or multiple), shape (round/oval or irregular), boundary (well-defined, partially ill-defined, or ill-defined); and (iii) the CT value of the HyS: on plain and contrast-enhanced CT images acquired at the same session, the similar region of interest was placed on the HyS at the same location and section for measuring. The blood vessels, gas, and bulkhead structures were avoided. The measurement was repeated 3 times, and the mean value was taken as the CT value of the HyS. The enhancement of the HyS (ΔCT) was calculated by the following formula: ΔCT = peak CT value measured on enhanced images − CT value measured on plain CT scan.

Statistical analysis

The software SPSS 21.0 (IBM Corp., Armonk, NY, USA) and MedCalc (MedCalc Software, Ostend, Belgium) were used for statistical analyses. Continuous data and categorical variables were expressed as mean ± standard deviation and numbers and percentages, respectively. The Student's *t*-test was used to compare age, lesion size, and the CT value of the HyS between patients with ILs and MLs. The smoking amount comparison was performed using the Mann-Whitney U test. The Pearson's chi-square test and Fisher's exact test were used for comparing the frequency of clinical features, laboratory indicators, and CT characteristics between patients with ILs and MLs. Logistic regression analysis was performed to construct models for predicting ILs based on parameters with statistical differences. The CT value of the HyS and the prediction of the model were analyzed using the receiver operating characteristic (ROC) curve. The area under the curve (AUC) of different models was evaluated with the Delong test. A P value of <0.05 was considered statistically significant.

Results

Clinical and laboratory characteristics

The clinical data and laboratory examination results of patients with ILs and MLs are summarized in *Table 1*. Among them, there were 235 (54.27%) patients with 236 (54.25%) MLs, including 158 (66.95%) adenocarcinomas, 74 (31.36%) squamous cell carcinomas, and 3 (1.27%) adenosquamous cell carcinomas. Regarding the pathological findings of 199 ILs, 171 (85.93%) cases showed significant fibrous tissue hyperplasia and massive acute (neutrophils) or chronic (lymphocytes, macrophages) inflammatory cells infiltration accompanied by hyaloid degeneration, foam cells, or lymphoid follicles. Pulmonary carnification caused by alveolar epithelial hyperplasia and local abscess was found in some lesions. The residual 28 (14.07%) cases showed granulomatous inflammation and caseous necrosis with or without positive acid-fast staining. Clinically, they were diagnosed as inflammatory pseudotumor (38, 19.10%), nonspecific inflammation (130, 65.33%), and tuberculosis (31, 15.58%). Compared with patients with MLs, those with ILs were younger. More patients had symptoms and elevated C-reactive protein, but fewer patients had abnormal tumor markers including cytokeratin fragment 19 (CYFRA21-1), carcinoembryonic antigen (CEA), and neuron-specific enolase (NSE) (all $P<0.05$).

HyS

On the plain scan and contrast-enhanced images, the

Table 1 Patients' clinical characteristics and laboratory results

Parameters	Patients with MLs (n=235)	Patients with ILs (n=198)	P value
Gender			0.820
Female	70 (29.79)	57 (28.79)	
Male	165 (70.21)	141 (71.21)	
Age (years)	60.54±9.31	55.25±10.67	<0.0001
Symptoms			
Cough	93 (39.57)	126 (63.64)	<0.0001
Expectoration	48 (20.43)	88 (44.44)	<0.0001
Phlegm with blood	29 (12.34)	42 (21.21)	0.013
Hemoptysis	14 (5.96)	19 (9.60)	0.155
Chest pain	33 (14.04)	34 (17.17)	0.370
Fever	4 (1.70)	7 (3.54)	0.227
No obvious symptoms	112 (47.66)	42 (21.21)	<0.0001
Concomitant basic diseases			
Hypertension	37 (15.74)	34 (17.17)	0.689
Diabetes	29 (12.34)	28 (14.14)	0.581
Malignant tumor	6 (2.55)	1 (0.51)	0.193
Tuberculosis	6 (2.55)	15 (7.58)	0.015
Other lung diseases	8 (3.40)	3 (1.52)	0.213
Family history of lung cancer			0.190
Present	10 (4.26)	4 (2.02)	
Absent	225 (95.74)	194 (97.98)	
Smoking history			0.120
Yes	149 (63.40)	111 (56.06)	
No	86 (36.60)	87 (43.94)	
Smoking amount (pack-years)	35.48±20.80	31.50±20.08	0.078
Main inflammatory markers			
Increased WBC count	22 (9.36)	23 (11.62)	0.304
Increased N count	33 (14.04)	33 (16.67)	0.449
Increased PLT	11 (4.68)	5 (2.53)	0.236
Increased CRP	9 (3.83)	18 (9.09)	0.024

Table 1 (*continued*)

Table 1 (*continued*)

Parameters	Patients with MLs (n=235)	Patients with ILs (n=198)	P value
Elevated tumor markers (number of patients with elevated indicators/number of patients tested)			
CYFRA21-1	75/123	24/100	<0.0001
CEA	41/124	4/101	<0.0001
NSE	24/116	6/95	0.003
SCC-Ag	25/108	12/94	0.057
ProGRP	10/97	9/77	0.772
CA19-9	9/25	8/16	0.375
CA72-4	2/2	2/7	0.167
SF	3/17	13/17	0.002
AFP	0/9	0/7	–

Data are expressed as n (%) or mean ± standard deviation. ML, malignant lesion; IL, inflammatory lesion; WBC, white blood cell; N, neutrophils; PLT, procalcitonin; CRP, C-reactive protein; CYFRA21-1, cytokeratin fragment 19; CEA, carcinoembryonic antigen; NSE, neuron-specific enolase; SCC-Ag, squamous cell carcinoma antigen; ProGRP, progastrin-releasing peptide; CA19-9, carbohydrate antigen 19-9; CA72-4, carbohydrate antigen 72-4; SF, serum ferritin; AFP, alpha-fetoprotein.

numbers of cases with a HyS detected on the standard mediastinal window and the narrow window were 35, 54, 123, and 125 in ILs and 8, 23, 66, and 68 in MLs, respectively. The HyS was more commonly detected in ILs than in MLs (62.81% *vs.* 28.81%, P<0.0001). On the plain CT images, the detection rates of the HyS on narrow mediastinal windows were higher than those on standard mediastinal windows (ILs: 43.20% *vs.* 28.00%, P=0.002; MLs: 32.4% *vs.* 11.76%, P=0.012) (*Figure 2*). Additionally, the detection rates of the HyS on contrast-enhanced images were higher than those on plain scan images (all P<0.05).

The CT features of the HyS in ILs and MLs are shown in *Table 2*. Compared with those in MLs, more HyS in ILs were single, round or oval, well-defined, and had lower enhancement (ΔCT) (all P<0.0001) (*Figures 3,4*). The ROC curve for the ΔCT value suggested the AUC was 0.702 [95% confidence interval (CI): 0.622 to 0.782; P<0.0001], and the optimal cut-off value of ΔCT for differentiating ILs and MLs was 9.5 HU (sensitivity, 60.3%; specificity, 80.0%).

CT manifestations of lesions

The CT manifestations of ILs and MLs are shown in *Table 3*. There were significant differences in shape, margin, and peripheral changes between ILs and MLs (all P<0.0001). Compared with those in MLs, pleural thickening was more frequent and enlargement of lymph nodes was less common in ILs (both P<0.05).

Logistic regression model

The regression models were constructed according to the CT manifestations of lesions and the HyS with statistical differences in 193 patients with a HyS (*Figure 5*). There were significant differences in the AUC between model A [AUC: 0.953, 95% CI: 0.913 to 0.978; sensitivity: 91.34%, specificity: 86.36%; positive predictive value (PPV): 92.80%, negative predictive value (NPV): 83.82%] and model B (AUC: 0.986, 95% CI: 0.957 to 0.997; sensitivity: 96.03%, specificity: 94.03%; PPV: 96.80%, NPV: 92.60%) (P=0.0027). Moreover, model B revealed that in lesions with a HyS, the ill-defined boundary of lesions [odds ratio (OR), 13.331; 95% CI: 1.356 to 131.092; P=0.026], peripheral fibrosis (OR, 22.167; 95% CI: 2.734 to 179.727; P=0.004), a well-defined HyS (OR, 102.716; 95% CI: 5.787 to 1823.012; P=0.002), and the ΔCT value of the HyS <9.5 HU (OR, 33.425; 95% CI: 5.224 to 213.848; P<0.0001) were independent indicators for predicting ILs.

Discussion

Inflammation and lung cancer are the main causes of pulmonary mass-like lesions. The clinical and laboratory data of patients could provide some information for

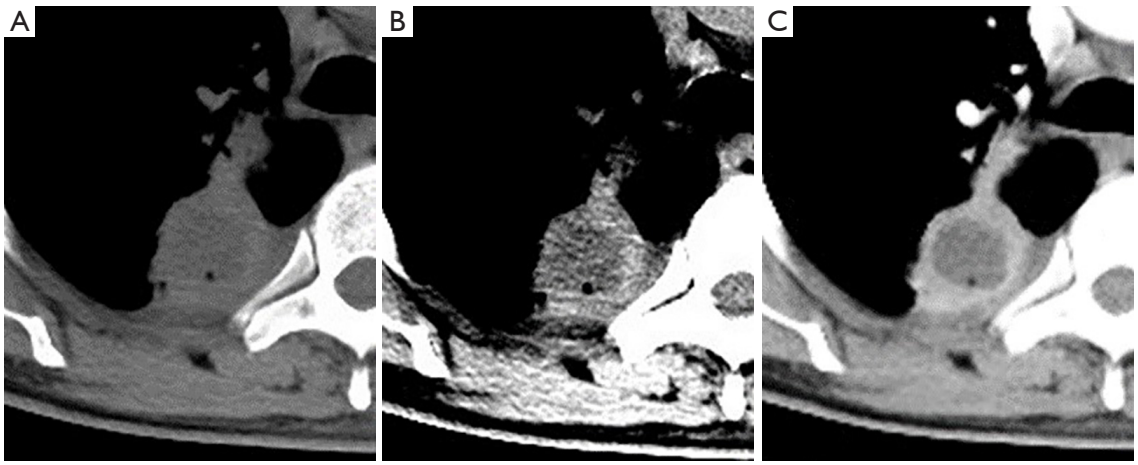

Figure 2 HyS on plain and contrast-enhanced CT scans. The plain CT scan shows a round and well-defined mass in the right lower lobe with pleural thickening; an ill-defined focal area with slightly lower attenuation; and a small vacuole is detected in the mass on standard mediastinal window (A), but it is clearer on the narrow mediastinal window (B). A well-defined and round HyS with ΔCT of 3.5 HU can be observed on the contrast-enhanced image (C). Pathologically, it consists of significant fibrous tissue and massive chronic inflammatory cells accompanied by localized abscess. ΔCT = peak CT value measured on enhanced images – CT value measured on plain CT scan. CT, computed tomography; HyS, hypodense sign; HU, Hounsfield units.

Table 2 CT characteristics of the HyS as depicted on CT in ILs and MLs

CT features	HyS in MLs (n=68)	HyS in ILs (n=125)	P value
Number			<0.0001
1	24 (35.29)	80 (64.00)	
>1	44 (64.71)	45 (36.00)	
Shape			<0.0001
Round/oval	21 (30.88)	95 (76.00)	
Irregular	47 (69.12)	30 (24.00)	
Boundary			<0.0001
Well-defined	11 (16.17)	89 (71.20)	
Partially ill-defined	31 (45.59)	25 (20.00)	
Ill-defined	26 (38.24)	11 (8.80)	
CT value on plain CT scan (HU)	17.25±10.23	16.36±12.08	0.607
CT value on enhanced CT scan (HU)	29.90±13.64	23.18±12.87	0.001
ΔCT (HU)	12.64±9.13	6.82±6.69	<0.0001

Data are expressed as n (%) or mean ± standard deviation. ΔCT = peak CT value measured on enhanced images – CT value measured on plain CT scan. CT, computed tomography; ML, malignant lesion; IL, inflammatory lesion; HyS, hypodense sign; HU, Hounsfield units.

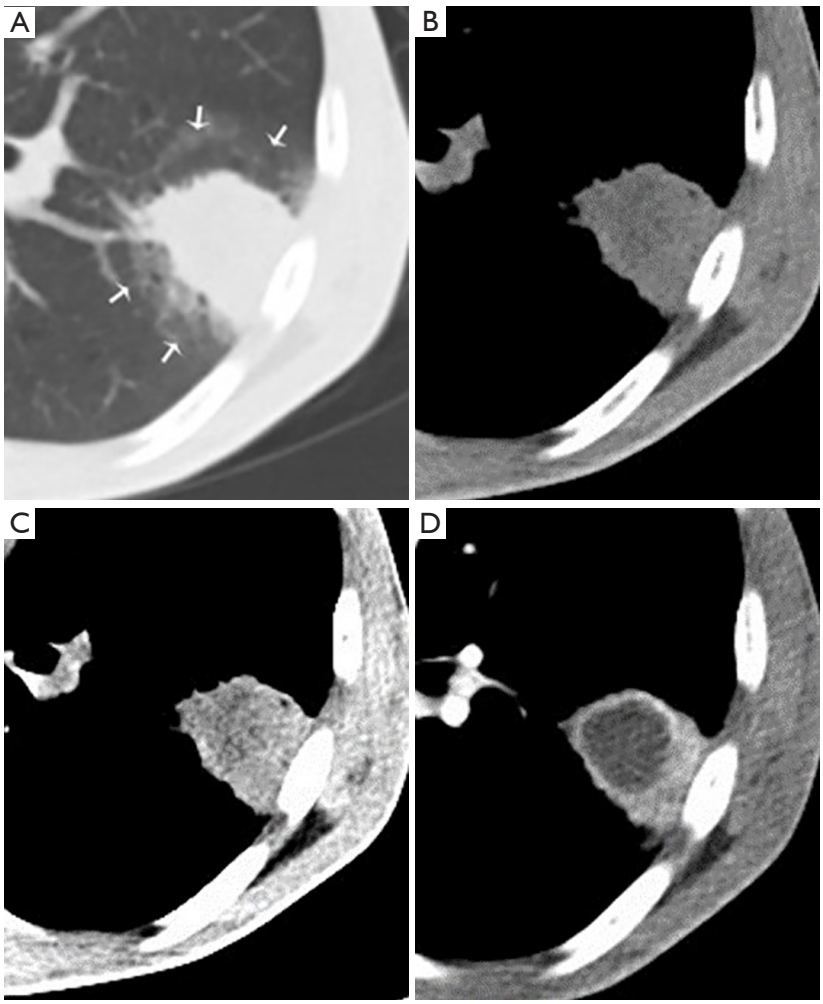

Figure 3 CT images of an inflammatory lesion. The plain CT scan shows an oval and well-defined mass with a halo sign (white arrow) in the left lower lobe (A); and an ill-defined focal area with slightly lower attenuation is detected in the mass on standard and narrow mediastinal window (B,C). A well-defined, and round HyS with ΔCT of 5.0 HU can be observed on the contrast-enhanced image (D). ΔCT = peak CT value measured on enhanced images – CT value measured on plain CT scan. CT, computed tomography; HyS, hypodense sign; HU, Hounsfield units.

differentiating ILs and MLs , but they were nonspecific. In this study, patients in both groups had similar clinical symptoms except for age differences. In terms of tumor biomarkers, more elevated CYFRA21-1, CEA, and NSE were found in patients with lung cancers, but some ILs also showed an increased level of these biomarkers. So far, no ideal tumor marker has been found, and a single abnormal index lacks sufficient sensitivity and specificity; a combination of multiple indicators is usually required (21-23). Moreover, the misdiagnosis rate of pulmonary ILs in patients without obvious clinical symptoms is extremely high (24). Therefore, a further noninvasive examination is necessary for diagnosing and differentiating pulmonary lesions.

As the most effective method in lung cancer detection (25,26), CT examination has a vital impact on the patients' treatment and prognosis. It can intuitively reflect similar or different manifestations of lesions caused by a different pathological process. Due to the exudation and fibroplasias, ill-defined boundaries and peripheral changes were more common in ILs than in MLs in our study (27-29). In contrast, more MLs in our study had lobulation and spiculation due to the variations in differentiation and growth rate of cancer cells and the contraction of internal

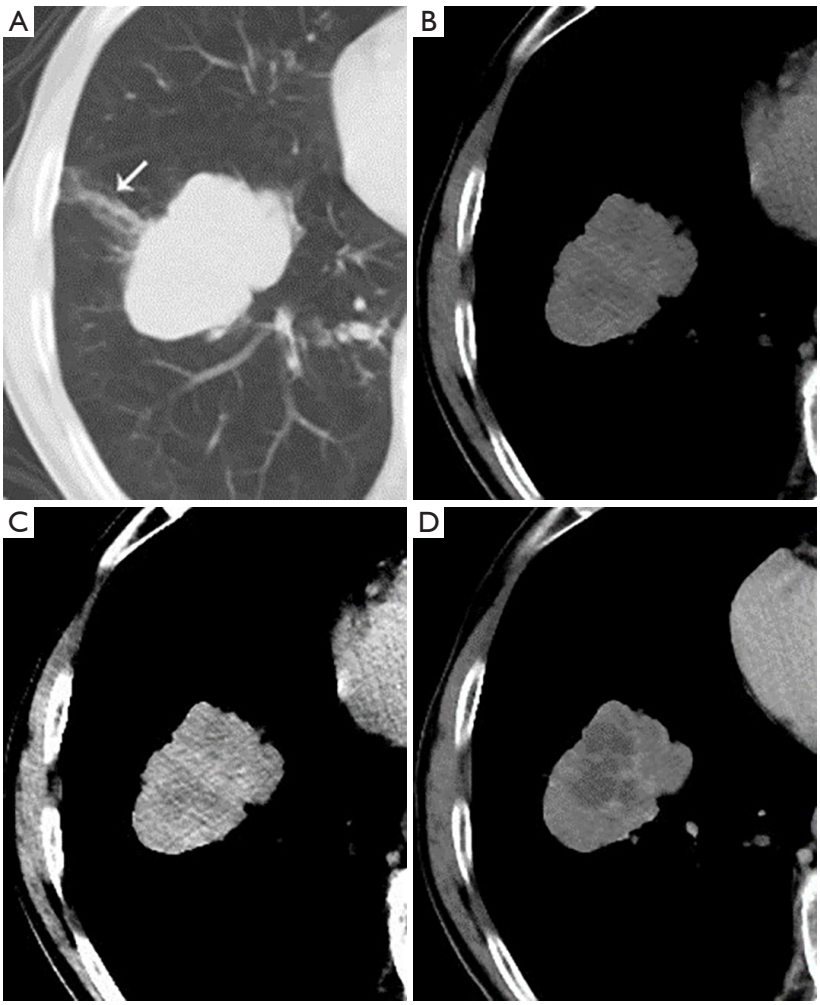

Figure 4 CT images of a malignant lesion. The plain CT scan shows a lobulated and well-defined mass with a beam-shaped opacity (white arrow) in the right lower lobe (A); and multiple ill-defined focal areas with slightly lower attenuation are detected in the mass on standard and narrow mediastinal window (B,C). Multiple, partially ill-defined, and irregular HyS with ΔCT of 10.2 HU can be observed on the contrast-enhanced image (D). ΔCT = peak CT value measured on enhanced images – CT value measured on plain CT scan. CT, computed tomography; HyS, hypodense sign; HU, Hounsfield units.

fibers. Additionally, our team previously found that beam-shaped opacity was commonly detected in peripheral lung cancer (15,16), which also applies to the present study. At the same time, the opacities around ILs were mainly patchy. Both lymph node metastasis and inflammatory reactive hyperplasia can cause hilar or mediastinal lymph node enlargement (30,31), leading to a limitation of CT in evaluating lymph node and tumor N staging (32,33). Therefore, even if the proportion of lymph node enlargement in ILs and MLs is different, its diagnostic and differential ability is limited.

The HyS is rarely mentioned when differentiating ILs and MLs. Generally, in an active fungal infection, the fungi infiltrate the adjacent pulmonary artery, leading to thrombosis and infarction, and proliferate rapidly through the hemorrhagic and infarcted lung, eventually forming a round expanded infarction, which appears as a central hypodense area of lesions on CT images (34). However, although it is a different pathological process, in non-fungal diseases, the central liquefaction in some active inflammations and the ischemic necrosis in tumors caused by the insufficiency of blood supply could also be shown as a CT HyS (35-37). The present study revealed that the occurrence of the HyS in ILs was significantly higher

Table 3 The CT findings of malignant and inflammatory lesions

CT manifestations	MLs (n=236)	ILs (n=199)	P value
Size (mm)	38.00±11.65	36.21±10.07	0.090
Location			0.239
Right upper lobe	102 (43.22)	65 (32.66)	
Right middle lobe	11 (4.66)	12 (6.03)	
Right lower lobe	42 (17.80)	44 (22.11)	
Left upper lobe	49 (20.76)	44 (22.11)	
Left lower lobe	32 (13.56)	34 (17.09)	
Shape			
Patchy	12 (5.08)	75 (37.69)	<0.0001
Round/oval	33 (13.98)	98 (49.25)	<0.0001
Lobulated	180 (76.27)	22 (11.06)	<0.0001
Irregular	11 (4.66)	4 (2.01)	0.131
Margin			
Smooth	61 (25.85)	30 (15.08)	0.006
Spiculated	155 (65.68)	67 (33.67)	<0.0001
Unclear	20 (8.47)	102 (51.26)	<0.0001
Peripheral changes			
GGO	136 (57.63)	100 (50.25)	0.124
Fibrosis	39 (16.53)	103 (51.76)	<0.0001
Halo sign	10 (4.24)	22 (11.06)	0.007
Nodule	2 (0.85)	20 (10.05)	<0.0001
Consolidation	7 (2.97)	0	0.039
Pleural changes			
Pleural traction	130 (55.08)	42 (21.11)	<0.0001
Pleural thickening	68 (28.81)	113 (56.78)	<0.0001
Enlarged lymph nodes			
Mediastinal lymph nodes enlargement	73 (30.93)	42 (21.11)	0.021
Hilar lymph nodes enlargement	78 (33.05)	40 (20.10)	0.002

Data are expressed as n (%) or mean ± standard deviation. CT, computed tomography; ML, malignant lesion; IL, inflammatory lesion; GGO, ground-glass opacity.

than that in MLs, which may be related to the abundant blood supply in active inflammation and the relatively slow growth of tumors with continuous neovascularization. Additionally, because of the setting of a narrow window and the application of a contrast agent, the contrast between a HyS and its surrounding tissues was enhanced, which improved the detection of the HyS. These findings were consistent with previous results (18,38). Given the significant differences in detection rates of the HyS on different images, CECT scan is necessary for diagnosing pulmonary mass-like lesions.

Although the HyS could be detected in both ILs and

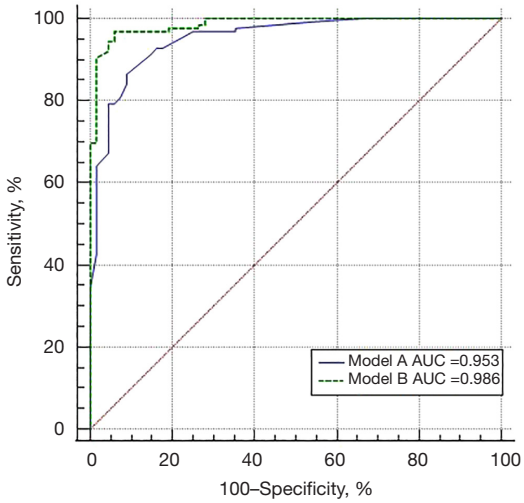

Figure 5 ROC curve for different regression models in predicting ILs (Model A: CT features of lesions excluding HyS; Model B: CT features of lesions including HyS). AUC, area under the curve; ROC, receiver operating characteristic; CT, computed tomography; ILs, inflammatory lesions; HyS, hypodense sign.

MLs, their CT characteristics had some differences. Most HyS in ILs were single, round or oval, and well-defined. In contrast, HyS in lung cancers were usually multiple, irregular, and ill-defined, which may be because of randomness, multifocality, and incomplete necrosis caused by hypoxia (39). On contrast-enhanced images, the incomplete necrosis areas in MLs may be enhanced more or less because of the residual tumor tissue, which causes the ΔCT values of the HyS in MLs to be higher than those in ILs. The ROC curve showed that lesions with ΔCT of the HyS <9.5 HU were likely to be ILs. Therefore, evaluating the CT features of the HyS is beneficial for distinguishing ILs from MLs, especially for those without significant morphological features.

Regarding the models for predicting ILs among the patients with the HyS, we found that the model combining the HyS and CT morphological features could improve the predictive performance of the model that solely considered CT morphological features. When a round and a well-defined HyS with enhancement less than 9.5 HU is detected in an ill-defined mass-like lesion, IL should be firstly considered even if the patient has no obvious clinical symptoms. Conversely, a lobulated, spiculated mass with beam-shaped opacity and internal irregular and an ill-defined HyS may be malignant, and further examination is needed.

The limitations of this study are as follows: first, this was a single-center retrospective study, and a prospective study is needed for our further verification. Second, different scanning parameters may lead to differences in CT value measurements; we matched patients with lung cancers according to the time period to eliminate this effect. Third, the exact causes of some ILs cannot be determined due to the nature of the retrospective study.

In conclusion, the HyS was more commonly detected in ILs, which manifested as pulmonary mass-like lesions. The CT features of the HyS can be used for distinguishing ILs from lung cancers. On CECT, a single, regular, and well-defined HyS with a ΔCT value of <9.5 HU in a pulmonary mass is highly suggestive of ILs. Combining the HyS with other morphological features could improve the diagnosis accuracy of pulmonary mass-like lesions.

Acknowledgments

Funding: This work was supported by the Joint Project Chongqing Science and Technology Commission and Chongqing Public Health Commission (No. 2022MSXM050) and Senior Medical Talents Program of Chongqing for Young and Middle-aged from Chongqing Health Commission (to Zhigang Chu).

Footnote

Reporting Checklist: The authors have completed the STARD reporting checklist. Available at https://qims.amegroups.com/article/view/10.21037/qims-21-851/rc

Conflicts of Interest: All authors have completed the ICMJE uniform disclosure form (available at https://qims.amegroups.com/article/view/10.21037/qims-21-851/coif). The authors have no conflicts of interest to declare.

Ethical Statement: The authors are accountable for all aspects of the work in ensuring that questions related to the accuracy or integrity of any part of the work are appropriately investigated and resolved. The study was conducted in accordance with the Declaration of Helsinki (as revised in 2013). This study was approved by the Ethics Committee of the First Affiliated Hospital of Chongqing Medical University (No. 2019-062). Individual consent for this retrospective analysis was waived.

Open Access Statement: This is an Open Access article

References

1. Barta JA, Powell CA, Wisnivesky JP. Global Epidemiology of Lung Cancer. Ann Glob Health 2019;85:8.
2. Siegel RL, Miller KD, Jemal A. Cancer statistics, 2019. CA Cancer J Clin 2019;69:7-34.
3. Bray F, Ferlay J, Soerjomataram I, Siegel RL, Torre LA, Jemal A. Global cancer statistics 2018: GLOBOCAN estimates of incidence and mortality worldwide for 36 cancers in 185 countries. CA Cancer J Clin 2018;68:394-424.
4. Jiang B, Takashima S, Miyake C, Hakucho T, Takahashi Y, Morimoto D, Numasaki H, Nakanishi K, Tomita Y, Higashiyama M. Thin-section CT findings in peripheral lung cancer of 3 cm or smaller: are there any characteristic features for predicting tumor histology or do they depend only on tumor size? Acta Radiol 2014;55:302-8.
5. Pecot CV, Li M, Zhang XJ, Rajanbabu R, Calitri C, Bungum A, Jett JR, Putnam JB, Callaway-Lane C, Deppen S, Grogan EL, Carbone DP, Worrell JA, Moons KG, Shyr Y, Massion PP. Added value of a serum proteomic signature in the diagnostic evaluation of lung nodules. Cancer Epidemiol Biomarkers Prev 2012;21:786-92.
6. Veronesi G, Bellomi M, Scanagatta P, Preda L, Rampinelli C, Guarize J, Pelosi G, Maisonneuve P, Leo F, Solli P, Masullo M, Spaggiari L. Difficulties encountered managing nodules detected during a computed tomography lung cancer screening program. J Thorac Cardiovasc Surg 2008;136:611-7.
7. Smith MA, Battafarano RJ, Meyers BF, Zoole JB, Cooper JD, Patterson GA. Prevalence of benign disease in patients undergoing resection for suspected lung cancer. Ann Thorac Surg 2006;81:1824-8; discussion 1828-9.
8. Snoeckx A, Reyntiens P, Desbuquoit D, Spinhoven MJ, Van Schil PE, van Meerbeeck JP, Parizel PM. Evaluation of the solitary pulmonary nodule: size matters, but do not ignore the power of morphology. Insights Imaging 2018;9:73-86.
9. Silvestri GA, Tanoue LT, Margolis ML, Barker J, Detterbeck F; American College of Chest Physicians. The noninvasive staging of non-small cell lung cancer: the guidelines. Chest 2003;123:147S-56S.
10. Mohamed Hoesein FA, Bülbül M, de Jong PA. Pulmonary nodule follow-up: be careful with volumetry between contrast enhanced and unenhanced CT. Ann Transl Med 2016;4:346.
11. Bhalla AS, Das A, Naranje P, Irodi A, Raj V, Goyal A. Imaging protocols for CT chest: A recommendation. Indian J Radiol Imaging 2019;29:236-46.
12. Li WJ, Lv FJ, Tan YW, Fu BJ, Chu ZG. Benign and malignant pulmonary part-solid nodules: differentiation via thin-section computed tomography. Quant Imaging Med Surg 2022;12:699-710.
13. Digumarthy SR, Padole AM, Lo Gullo R, et al. CT texture analysis of histologically proven benign and malignant lung lesions. Medicine (Baltimore) 2018;97:e11172.
14. Suo S, Cheng J, Cao M, et al. Assessment of Heterogeneity Difference Between Edge and Core by Using Texture Analysis: Differentiation of Malignant From Inflammatory Pulmonary Nodules and Masses. Acad Radiol 2016;23:1115-22.
15. Chu ZG, Sheng B, Liu MQ, Lv FJ, Li Q, Ouyang Y. Differential Diagnosis of Solitary Pulmonary Inflammatory Lesions and Peripheral Lung Cancers with Contrast-enhanced Computed Tomography. Clinics (Sao Paulo) 2016;71:555-61.
16. Chu ZG, Zhang Y, Li WJ, Li Q, Zheng YN, Lv FJ. Primary solid lung cancerous nodules with different sizes: computed tomography features and their variations. BMC Cancer 2019;19:1060.
17. Horger M, Einsele H, Schumacher U, Wehrmann M, Hebart H, Lengerke C, Vonthein R, Claussen CD, Pfannenberg C. Invasive pulmonary aspergillosis: frequency and meaning of the "hypodense sign" on unenhanced CT. Br J Radiol 2005;78:697-703.
18. Sassi C, Stanzani M, Lewis RE, Facchini G, Bazzocchi A, Cavo M, Battista G. The utility of contrast-enhanced hypodense sign for the diagnosis of pulmonary invasive mould disease in patients with haematological malignancies. Br J Radiol 2018;91:20170220.
19. Stanzani M, Sassi C, Lewis RE, Tolomelli G, Bazzocchi A, Cavo M, Vianelli N, Battista G. High resolution computed tomography angiography improves the radiographic diagnosis of invasive mold disease in patients with hematological malignancies. Clin Infect Dis 2015;60:1603-10.
20. Fukukura Y, Kumagae Y, Fujisaki Y, Yamagishi R,

Nakamura S, Kamizono J, Nakajo M, Kamimura K, Nagano H, Takumi K, Yoshiura T. Adding Delayed Phase Images to Dual-Phase Contrast-Enhanced CT Increases Sensitivity for Small Pancreatic Ductal Adenocarcinoma. AJR Am J Roentgenol 2021;217:888-97.
21. Grunnet M, Sorensen JB. Carcinoembryonic antigen (CEA) as tumor marker in lung cancer. Lung Cancer 2012;76:138-43.
22. Chen ZQ, Huang LS, Zhu B. Assessment of Seven Clinical Tumor Markers in Diagnosis of Non-Small-Cell Lung Cancer. Dis Markers 2018;2018:9845123.
23. Chen F, Li J, Qi X, Qi J. Diagnostic value of CYFRA 21-1 and carcinoembryonic antigen in diagnosis of operable lung cancer from benign lung disease. J Cancer Res Ther 2018;14:S400-4.
24. Hong SJ, Kim TJ, Lee JH, Park JS. Nontuberculous mycobacterial pulmonary disease mimicking lung cancer: Clinicoradiologic features and diagnostic implications. Medicine (Baltimore) 2016;95:e3978.
25. Thakur SK, Singh DP, Choudhary J. Lung cancer identification: a review on detection and classification. Cancer Metastasis Rev 2020;39:989-98.
26. Beigelman-Aubry C, Dunet V, Brun AL. CT imaging in pre-therapeutic assessment of lung cancer. Diagn Interv Imaging 2016;97:973-89.
27. Huang CC, Hung ST, Chang WC, Sheu CY. Benign features of infection-related tumor-like lesions of the lung: A retrospective imaging review study. J Med Imaging Radiat Oncol 2017;61:481-8.
28. Zhang X, Lv F, Fu B, Li W, Lin R, Chu Z. Clinical and Computed Tomography Characteristics for Early Diagnosis of Peripheral Small-cell Lung Cancer. Cancer Manag Res 2022;14:589-601.
29. He XQ, Li X, Wu Y, Wu S, Luo TY, Lv FJ, Li Q. Differential Diagnosis of Nonabsorbable Inflammatory and Malignant Subsolid Nodules with a Solid Component ≤5 mm. J Inflamm Res 2022;15:1785-96.
30. Silvestri GA, Gonzalez AV, Jantz MA, Margolis ML, Gould MK, Tanoue LT, Harris LJ, Detterbeck FC. Methods for staging non-small cell lung cancer: Diagnosis and management of lung cancer, 3rd ed: American College of Chest Physicians evidence-based clinical practice guidelines. Chest 2013;143:e211S-50S.
31. Liam CK, Andarini S, Lee P, Ho JC, Chau NQ, Tscheikuna J. Lung cancer staging now and in the future. Respirology 2015;20:526-34.
32. Gelberg J, Grondin S, Tremblay A. Mediastinal staging for lung cancer. Can Respir J 2014;21:159-61.
33. Rami-Porta R, Call S, Dooms C, Obiols C, Sánchez M, Travis WD, Vollmer I. Lung cancer staging: a concise update. Eur Respir J 2018;51:1800190.
34. Kang EY, Kim DH, Woo OH, Choi JA, Oh YW, Kim CH. Pulmonary aspergillosis in immunocompetent hosts without underlying lesions of the lung: radiologic and pathologic findings. AJR Am J Roentgenol 2002;178:1395-9.
35. Bayanati H, E Thornhill R, Souza CA, Sethi-Virmani V, Gupta A, Maziak D, Amjadi K, Dennie C. Quantitative CT texture and shape analysis: can it differentiate benign and malignant mediastinal lymph nodes in patients with primary lung cancer? Eur Radiol 2015;25:480-7.
36. Ganeshan B, Goh V, Mandeville HC, Ng QS, Hoskin PJ, Miles KA. Non-small cell lung cancer: histopathologic correlates for texture parameters at CT. Radiology 2013;266:326-36.
37. Gkogkou C, Frangia K, Saif MW, Trigidou R, Syrigos K. Necrosis and apoptotic index as prognostic factors in non-small cell lung carcinoma: a review. Springerplus 2014;3:120.
38. Schulze M, Vogel W, Spira D, Sauter A, Hetzel J, Horger M. Reduced perfusion in pulmonary infiltrates of high-risk hematologic patients is a possible discriminator of pulmonary angioinvasive mycosis: a pilot volume perfusion computed tomography (VPCT) study. Acad Radiol 2012;19:842-50.
39. Davnall F, Yip CS, Ljungqvist G, Selmi M, Ng F, Sanghera B, Ganeshan B, Miles KA, Cook GJ, Goh V. Assessment of tumor heterogeneity: an emerging imaging tool for clinical practice? Insights Imaging 2012;3:573-89.

Cite this article as: Fu BJ, Lv ZM, Lv FJ, Li WJ, Lin RY, Chu ZG. Sensitivity and specificity of computed tomography hypodense sign when differentiating pulmonary inflammatory and malignant mass-like lesions. Quant Imaging Med Surg 2022;12(9):4435-4447. doi: 10.21037/qims-21-851

